A Novel Calibration Method for Industrial AGVs

Fabjan Kallasi[a], Dario Lodi Rizzini[a], Fabio Oleari[a,b], Massimiliano Magnani[b], Stefano Caselli[a]

[a] *Robotics and Intelligent Machines Laboratory, Department of Information Engineering, University of Parma, 43124, Italy*
[b] *Elettric80 S.p.A. 42030 Viano (RE), Italy*

Abstract

We propose a novel calibration method for industrial Automated Guided Vehicles (AGVs) adopting the tricycle wheeled robot model and equipped with an on-board exteroceptive sensor. The method simultaneously estimates the calibration parameters for the odometry and the exteroceptive sensor using only the input commands and the sensor egomotion of the robot while executing segment paths. Two AGV models, both relevant to industrial practice, are considered: the standard tricycle model and an asymmetric one that takes into account the different weight distribution in forward and backward motions typical of industrial AGVs. The parameters of the standard model comprise the steering offset and driving scale, which measure the angular offset of the tricycle steering wheel and the distance increment corresponding to an encoder tick, and the three parameters representing the sensor pose. The asymmetric model adopts different values for the steering offset in forward and backward motions to account for the different weight distribution. Closed-form or compact solutions are provided for both problem formulations. The observability of the calibration procedure is also formally proved. The proposed automated calibration procedure has been implemented on industrial AGVs, leading to estimation of the parameters in about 12 minutes, a significant improvement compared with one hour or more required by manual AGV calibration. Experiments with AGVs of various sizes in warehouses have assessed the effectiveness and numerical stability of the proposed approach. The precision of calibration parameters has been found to be about 0.1° for angles and 6 mm for positions. Parameters obtained via the proposed automated calibration procedure have allowed different AGVs to accurately stop at the desired operation points.

Keywords: Industrial mobile robots, extrinsic calibration, odometry calibration.

1. Introduction

A common requirement of industrial robotic systems is the capability to repeat operations with adequate precision. Precision is a fundamental requirement of traditional assembly lines where products are moved by robot manipulators and other devices, as well as of warehouse logistic systems exploiting *automated guided vehicles* (AGVs). AGVs are mobile robots equipped with forks or other grasping devices to transport pallets and materials from a warehouse location to another according to assigned production policies. Since the exact location of each pallet is registered into a database, AGVs estimate their pose using an exteroceptive sensor, often a navigation range finder and artificial reflectors, to accurately pick and drop items. Figure 1 shows a typical AGV in an industrial setting.

The accuracy of robotic systems depends on the estimation of parameters that describe their motion and configuration. These parameters either represent the robot internal state or relate other sensors or devices to the robot. Respectively, the former are called *intrinsic parameters* and the latter *extrinsic parameters*. Intrinsic parameters usually describe the relationship between the actuators state and the robot kinematics. Extrinsic parameters relate the sensor measurements to the robot reference frame. The correct assessment of the AGV parameters affects its navigation accuracy, namely its odometry and localization. Hence, the aim of calibration is the accurate estimation of these parameters.

A standard approach for mobile robot calibration is to compare the expected motion of the robot from some input commands with the observed trajectory. Currently, industrial vehicles are calibrated through a manual procedure requiring the intervention of an operator to measure the effective trajectory. Each parameter is updated in sequence and multiple iterations are often needed. This is a tedious process requiring at least one hour for each AGV. Its accuracy largely depends on the skills and experience of the operator performing the calibration. Moreover, consistency of manual calibration with multiple, possibly different AGVs operating in the same warehouse is often questionable and can lead to AGVs exhibiting slightly different behavior for the same nominal position.

Since AGVs are usually equipped with one or more sensors for localization and navigation (e.g. a laser scanner) that can estimate the sensor egomotion, on-board sensors can be used to estimate the effective motion of the vehicle. Knowledge of the relative pose of the on-board sensor w.r.t. the robot frame is required to obtain the real robot trajectory using such sensor. The sensor relative pose can be assessed from its egomotion while the robot moves on a known trajectory. Thus, a completely automated calibration method should estimate both intrinsic and extrinsic parameters. A more efficient and accurate procedure can bring remarkable improvements to industrial applications, including the faster setup of an AGV fleet and the possibility for less expensive and more frequent recalibration to compensate parameter changes over time due to mechanical wear, vibrations, and collisions.

Research has addressed several formulations of calibration problems for different robotic systems, including the calibration of multi-sensor systems and robot odometry [1, 2, 3, 4, 5, 6, 7, 8, 9, 10, 11, 12, 13, 14, 15, 16, 17, 18, 19, 20, 21, 22, 23, 24, 25, 26, 27, 28]. Many works focus on the estimation of either intrinsic [2, 3, 4, 5, 6, 7, 29, 8, 9, 10, 11, 23, 24, 25] or extrinsic parameters [12, 13, 14, 15, 16, 17, 18, 19, 20, 21, 22, 26, 27, 28]. Recently, an algorithm for the complete calibration of a mobile robot has been proposed [1]. The kinematic model considered in works addressing mobile robot calibration [1, 2, 3, 4, 5, 6, 7, 10, 11] is the popular differential drive. The proposed techniques therefore are mostly suited for a laboratory robotic platform rather than industrial vehicles, since AGVs seldom adopt such kinematic configuration. Furthermore, these approaches do not take into account practical and numerical issues arising in industrial setups. Indeed, AGVs operate in large scale environments where odometric errors due to long travelled distances do occur. Moreover, AGVs are usually designed according to a *tricycle structure* consisting of a steering actuated front wheel and two passive back wheels, due the simplicity of such self-standing configuration as well as its suitability for fetching, carrying, and depositing heavy loads. The tricycle robot, which is kinematically equivalent to a bicycle [29, p. 482], has been largely ignored in the investigation of calibration. To our knowledge, no approach has addressed so far automatic calibration of both intrinsic and extrinsic parameters of tricycle robots equipped with a sensor.

In this paper, we present the first method for simultaneous intrinsic and extrinsic calibration of tricycle robots equipped with a sensor like a planar laser scanner. Parameter estimation is achieved by comparing the motion expected from kinematic equations and the sensor egomotion. Two differ-

Figure 1: An industrial AGV (Elettric80 CB25) equipped with a navigation laser scanner at the top of a telescopic pole.

ent kinematic models have been investigated: the standard tricycle model and an asymmetric model taking into account the different load conditions affecting the wheel steer axis when a real industrial AGV moves forward and backward. Closed-form solutions have been derived for both calibration formulations. Moreover, the correctness of the proposed algorithm has been formally assessed by stating observability conditions on input trajectories. In order to cope with uncertainty and errors in measurements it is important to check the accuracy of the estimated values at increasing level of noise. We assess the motion constraints under which the calibration method results into a well-conditioned problem.

The method has been implemented on the control system of industrial AGVs using the native language of Programmable Logic Controllers (PLC) compliant with IEC-61131-3. PLC-like systems are commonly used in industrial applications due to strong real-time requirements and need to interface with sensors and devices, but the associated programming language usually lacks the support of libraries. The proposed algorithm can be straightforwardly developed for these systems thanks to its closed-form formulation. The implemented calibration procedure is completely automatic and does not require any intervention of the operator. Full estimation of calibration parameters is obtained in about 12 minutes, which is the time required by the

AGV to perform an adequate number of motions. Experiments performed in real industrial setups, including production warehouses, have shown that the values computed with the proposed method are stable and yield accurate AGV navigation capabilities.

2. Related Work

Calibration of mobile robots has been addressed from several points of view by academic research. Calibration may refer only to the estimation of the robot kinematic parameters used in odometry computation or may include the relationship between the robot and its sensors. During the last two decades, research has addressed the assessment of mobile robot intrinsic parameters, of the extrinsic parameters of a sensor mounted on it, or of both sets of parameters.

2.1. Manual Odometry Calibration

Most of odometry calibration literature is devoted to differential drive robots. Several wheeled mobile robots are designed with a differential drive actuation system due to the simplicity of such configuration. In particular, the parameters to be estimated are the two wheel diameters and the wheel-base distance. Borenstein et al. [2] likely proposed the first specific calibration method for differential drive robots, the *UMBmark*. This technique requires the robot to move along a square trajectory in both directions, clockwise and counterclockwise, and measures the displacement between the final and the starting points after the execution of a loop to compute the correction factors of wheel-base and wheel diameters. This approach has been applied also to other kinematic models such as the car-like [8] or the tricycle [9], but mainstream research has been focused on differential drive. Odometry calibration is coupled with the calibration of internal sensors like gyroscopes and IMUs used to correct odometry [9]. Currently, similar procedures are often used to estimate odometric parameters in industrial practice: the robot follows specific paths (typically straight lines or loops) and the distance between the expected path with initial parameters and the measured one is used to correct parameters. Such distance is measured either manually or through an external absolute positioning system. Moreover, each calibration parameter is estimated sequentially after performing a specific step, instead of performing a simultaneous optimization. The separate assessment of each parameter is usually less accurate.

2.2. Calibration based on Filtering Methods

In several works the calibration problem has been addressed using the same Bayesian filtering algorithms adopted for robot localization. The system state consists of both the robot pose and its kinematic parameters, although the latter do not change or slowly change over the time. Larsen et al. [3] and Martinelli et al. [5] present augmented Extended Kalman Filter (AEKF) algorithms that simultaneously localize and calibrate the mobile robot. The method illustrated in [10] jointly uses a gyroscope, the wheel encoders, and a GPS unit in a Kalman filter to correct systematic errors. In [11] a simultaneous SLAM and calibration algorithm specific for feature maps is presented. These works are designed for differential drive and, thus, cannot be applied to other drive models. Furthemore, they do not simultaneously estimate the intrinsic and extrinsic parameters.

Calibration of on-board sensors through EKF is a rather straightforward step. Extrinsic calibration parameters usually describe the pose of a sensor w.r.t. a common reference frame fixed on the robot. The EKF has been applied to the calibration of different kinds of sensors or of heterogeneous sensors. Early examples of camera calibration techniques based on Kalman filter can be found in [14], the latter specific for eye-in-hand cameras. The extrinsic parameters of laser scanners are estimated by tracking moving targets [15] or by comparing the robot pose evolution and the landmark measurements [16]. Foxlin [12] proposed a general EKF framework that allows localization and calibration of multiple sensors. Martinelli et al. [17] describe an EKF for assessing the parameters of a camera mounted on a robot during the robot motion. This work presents one of the first observability analysis for a calibration problem based on discrete-time system state evolution, which has been further developed in [4]. The authors also provide an observability analysis proving the formal correctness of the calibration process. Mirzaei and Roumeliotis [18] illustrate a method for calibrating a camera and an inertial sensor using a Kalman filter. The works discussed above are designed only to estimate the pose of one or more sensors w.r.t. the robot or to another sensor.

2.3. Calibration based on Least-square Optimization

Least square optimization has been used to estimate both intrinsic and extrinsic parameters. Historically, optimization is the earliest approach to specific calibration problems in robotics and computer vision like pinhole single and stereo cameras [13, 19] and eye-in-hand cameras [20, 21]. These

techniques usually compute a closed-form initial estimation based on a simplified model and next refine this estimation by numerically optimizing the error associated to more complex sensor models taking into account optical distortions, offsets, etc. Calibration of heterogeneous sensor systems requires a target that is observable from different sensor domains and geometries. Zhang and Pless [22] illustrate a method for a planar range finder and a camera exploiting a planar checkerboard.

In mobile robotics, the extrinsic or intrinsic calibration based on least-square optimization is more recent. Sometimes the function to be optimized is obtained from a stochastic formulation of the problem. Roy and Thrun [23] proposed the computation of the intrinsic parameters according to maximum likelihood criterion: the robot builds a map while moving, and estimates the likelihood function to be maximized. Antonelli et al. [6, 7] focus on the differential drive model and on the linear relationship between the observed robot motion and the quantities depending on intrinsic parameters. The calibration is achieved by solving a linear optimization problem and a bound on the calibration error is provided. An analysis of odometry error propagation is described in [24]. The work in [25] presents a calibration framework based on a graphical model formulation. The framework is rather general, but it does not explicitly consider the robot model and is potentially prone to convergence problems and inaccuracies. Underwood et al.[26] and Brookshire and Teller [27] address the calibration of multiple sensors mounted on a mobile robot using least-square optimization. The latter work has been extended from coplanar sensors to 3D range sensors like depth cameras [28].

The only complete odometry and sensor calibration method is reported in [1]. The estimation of intrinsic and extrinsic parameters is decoupled into two steps. The intrinsic calibration is the straightforward application of the differential drive solution [7]. The extrinsic parameters are obtained by comparing the robot motion and the sensor egomotion. The closed-form solution for extrinsic parameters proposed in [1] is dependent from the intrinsic calibration parameters. Such method cannot be used for the calibration of industrial AGVs, which are designed according to the tricycle kinematic model and not to the differential drive one.

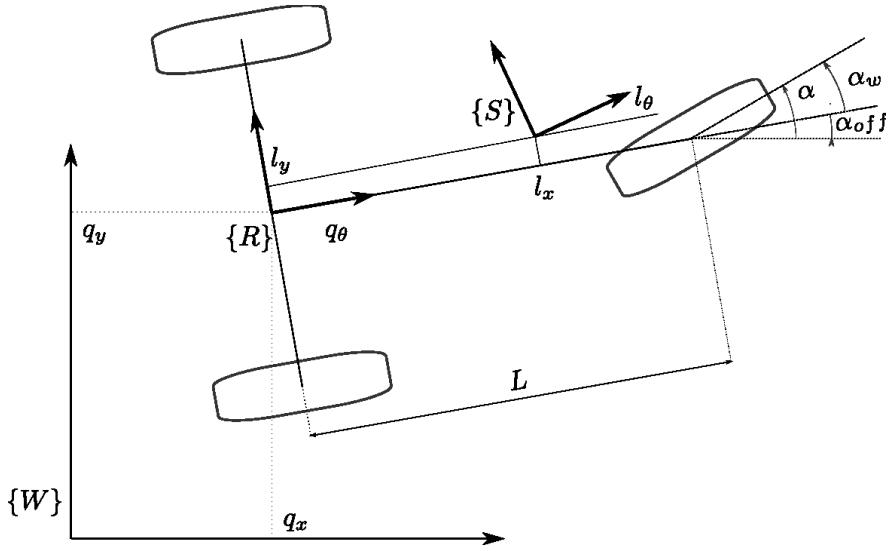

Figure 2: The tricycle model: $\{W\}$ world reference frame; $\{R\}$ robot frame in the robot logical point; $\{S\}$ sensor frame.

3. Problem Formulation

3.1. Standard Tricycle Model

The typical configuration of industrial AGVs is the tricyle wheeled robot model, which comprises three wheels and is also self-standing. The front wheel, also called *driving wheel*, is actuated and controlled by setting its steering angle and velocity. The two back wheels are coaxial, i.e. their rotation axis is the same, and passive. The robot reference frame $\{R\}$ is placed on the orthogonal projection of the driving wheel center on the back axis. This reference frame is also called *logical point*, since the pose and velocities of the whole are logically described by the kinematic state of the frame origin. Figure 2 illustrates the tricycle robot model. The robot is equipped with a sensor, which allows localization and egomotion estimation, and models the laser scanner usually mounted on industrial AGVs. The world reference frame $\{W\}$ is fixed in the environment. The sensor reference frame $\{S\}$ is rigidly mounted on the robot so that their relative pose is constant over time. Let $q = [q_x, q_y, q_\theta]^\top \in \mathrm{se}(2)$ be the state vector representing the position and orientation of reference frame $\{R\}$ w.r.t. the world frame $\{W\}$ and $l = [l_x, l_y, l_\theta]^\top$ be the constant relative pose of frame $\{S\}$ w.r.t. frame

$\{R\}$. The kinematic model that describes the evolution of state vector q over time is

$$\dot{q} = \begin{bmatrix} v_{lp} \ \cos(q_\theta) \\ v_{lp} \ \sin(q_\theta) \\ \omega_{lp} \end{bmatrix} \tag{1}$$

The state vector and all the variables that depend on time will be sometimes explicitly written as a function of time, i.e. $q(t)$. Although the linear and angular velocities v_{lp} and ω_{lp} are convenient to describe the motion of the logical point, the real controls for the tricycle robot are set on the front *steering wheel*, whose dynamic configuration is described by its linear velocity v_w and its steering angle α_w. The steering wheel state is controlled by two motors, one for rotating the wheel and the other for steering, and monitored by the corresponding encoders.

The distance travelled by the wheel is proportional to the *number of ticks* n_w counted by the driving encoder. The *driving scale* s_w is a constant that binds the distance travelled by the robot to the rotation of the wheel. The driving scale depends on the wheel radius (which changes in time as the wheel wears out), on the transmission gears, and on the angular resolution of the encoder. Hence, the wheel linear velocity v_w can be written as the product of the driving scale s_w and the derivative of tick number in time $\dot{n}_w$.

The robot rotation velocity depends on the *wheelbase* L, which is the distance between the origin of reference frame $\{R\}$ and the steering wheel axis, and on the steering angle α_w (see Figure 2). In industrial practice, the wheelbase is assumed to be accurately known from the mechanical design. The steering wheel direction for $\alpha_w = 0$ is orthogonal to the back wheel axis and the robot moves on a straight line. The encoder of the motor controlling the steer measures the *steering angle* α w.r.t. the encoder reference angle. Unfortunately, it is very difficult to mount the encoder such that its reference angle is perfectly aligned with the straight direction. Thus, there is a *steer offset* α_{off} between the measured steering angle α w.r.t. the reference angle and α_w, so that $\alpha_w = \alpha + \alpha_{off}$ as shown in Figure 2. Thus, the linear and angular velocities in equation (1) can be written as

$$v_{lp} = v_w \ \cos\alpha_w = s_w \ \dot{n}_w \ \cos(\alpha + \alpha_{off}) \tag{2}$$

$$\omega_{lp} = \frac{v_w \ \sin\alpha_w}{L} = \frac{s_w \ \dot{n}_w \ \sin(\alpha + \alpha_{off})}{L} \tag{3}$$

The range finder mounted on the robot is such that the scanning plane is parallel to the ground plane. Hence, the sensor pose $s(t)$ w.r.t. the world

reference frame $\{W\}$ is conveniently described by the robot pose $q(t)$ and the relative pose of the sensor $l = [l_x, l_y, l_\theta]^\top \in \mathrm{se}(2)$. The relationships between l, $q(t)$ and the other poses can be expressed using standard compounding and inversion operators on special Euclidean Lie algebra $\mathrm{se}(2)$, respectively $\oplus$ and $\ominus$ [30]. Furthermore, the symbol $\mathrm{R}(\cdot)$ refers, henceafter, both to the map from an angle $\beta \in S^1$ to the corresponding rotation matrix of $\mathrm{R}(\beta) \in \mathrm{SO}(2)$ and to the map from a vector $b \in \mathbb{R}^2$ to a skew matrix $\mathrm{R}(b) \in \mathbb{R}^{2\times 2}$ defined respectively as

$$\mathrm{R}(\beta) \triangleq \begin{bmatrix} \cos\beta & -\sin\beta \\ \sin\beta & \cos\beta \end{bmatrix}, \mathrm{R}(b) \triangleq \begin{bmatrix} b_x & -b_y \\ b_y & b_x \end{bmatrix} \tag{4}$$

This abuse of notation allows us to write compact formulas and to straightforwardly compute the expressions. The position of the sensor is then equal to $s(t) = q(t) \oplus l$. The measurement values of actuators and sensors are acquired at given sampling times $t_1, \ldots, t_k$.

The problem addressed in this paper is the estimation of the following parameters:

- *intrinsic parameters*: the driving scale of the wheel s_w, which relates the encoder ticks and the linear velocity, and the steering offset angle α_{off};
- *extrinsic parameters*: the laser scanner pose parameters $l = [l_x, l_y, l_\theta]^\top$.

The available data are the relative motions of the robot and the laser scanner frames at the sample times t_k with $k = 0, \ldots, n$. The choice of the number of samples is formally discussed in section 5 and experimentally assessed in section 6. In particular, the relative robot motion r^k corresponds to the relative motion of robot $\ominus q(t_{k-1}) \oplus q(t_k)$. The value of r^k depends on the controls and the intrinsic parameters of the robot; sometimes the notation $r^k(s_w, \alpha_{off})$ will emphasize the dependence from intrinsic parameters. The sensor relative pose between the two time instants t_{k-1} and t_k is called $s^k = [s^k_x, s^k_y, s^k_\theta]^\top$. We assume that s^k are measured or computed using the sensor measurements. The measurements r^k and s^k are constrained by the following relationship

$$l \oplus s^k = r^k \oplus l \tag{5}$$

Given a value of l, the difference between the first and second members of equation (5) represents the error on extrinsic parameters l related to the k-th measurements of s^k and r^k. The best estimation of l can be found by

minimizing a goal error function that could be defined as the sum of such square errors with $k = 1, \ldots, n$.

Definition 3.1 (Standard Tricycle Calibration, STC)**.** *Given the measured steering angle $\alpha(t)$ and the number of travelled encoder ticks n_w^k on interval $[t_{k-1}, t_k]$ with $k = 1, \ldots, n$, and the sensor egomotion $s^k = [s_x^k, s_y^k, s_\theta^k]^\top$ on each interval, a calibration algorithm computes the values of the intrinsic parameters α_{off} and s_w, and of extrinsic parameters $l = [l_x, l_y, l_\theta]^\top$.*

3.2. Asymmetric Tricycle Model

The parameter model given by equations (2) and (3) enables accurate estimation of robot motion for most applications. However, it does not fully model some peculiarities related to the mechanical structure or to the space geometry of the system. The model accuracy is compromised by mechanical clearance and friction, which are high in industrial AGVs like the one shown in Figure 1. In particular, the wheel steer axis is subject to torques, which are significantly different whether the robot moves forward or backward. Such difference is more clearly seen when the AGV carries a pallet using the bottom fork-lift. The different motion direction affects the value of the steering offset. For this reason, an *asymmetric model* with two different steer offsets α_F and α_B, respectively forward and backward steer offsets, has been developed. The asymmetry can be modelled by a piecewise function

$$\alpha_{off}(\dot{n}_w) = \begin{cases} \alpha_F & \text{if } \dot{n}_w > 0 \\ \alpha_B & \text{otherwise} \end{cases} \tag{6}$$

which can be substituted in equations (2) and (3). The new formulation has the disadvantage of a discontinuous value of α_{off}, but for our purposes the robot motion can be divided into segments of forward or backward motion with a single α_{off} value. Thus, a second formulation of the calibration problem can be given.

Definition 3.2 (Asymmetric Tricycle Calibration, ATC)**.** *Given the measured steering angle $\alpha(t)$ and the number of travelled encoder ticks n_w^k on interval $[t_{k-1}, t_k]$ with $k = 1, \ldots, n$, and the sensor egomotion $s^k = [s_x^k, s_y^k, s_\theta^k]^\top$ on each interval, a calibration algorithm computes the values of the intrinsic parameters α_F, α_B and s_w, and of extrinsic parameters $l = [l_x, l_y, l_\theta]^\top$.*

The solution of ATC problem is obtained from the same equations of STC problem, but using different constraints. Since the difference between

the two formulations lies in intrinsic parameters, the estimation of the sensor pose l is reasonably obtained using the same method.

4. Calibration Method

The calibration method proposed in this paper estimates both the intrinsic and extrinsic parameters by moving the robot with constant input controls. The hypothesis of constant input controls is not restrictive and yields simpler model equations while allowing accurate estimation of the robot motion. If its controls are constant, then a tricycle robot moves along circular path segments. The relative pose displacement of the sensor frame at the beginning and end of each path can be measured by the sensor egomotion. Such information within the control setpoints can be used to compute both the intrinsic and extrinsic parameters in two consecutive steps. First, the values of intrinsic parameters are estimated from odometry according to STC or ATC formulation. Second, the navigation sensor pose is computed by minimizing the square mismatch between robot motion and sensor egomotion.

4.1. Standard Intrinsic Calibration

The relative robot motion r^k on time interval $[t_{k-1}, t_k]$ is obtained by integrating the differential equation (1). It is convenient to relate the value of r^k with the kinematic variables α and $\dot{n}_w$ that represent the motion of the driving wheel. The linear and angular velocities of the logical point, respectively v_{lp} and ω_{lp}, depend from α and $\dot{n}_w$ according to the equations (2) and (3). The orientation and position can be straightforwardly obtained by a separated integration of the terms of equation (1) when the input control $\alpha(t)$ is constant on the time interval. Henceafter, the path travelled by the robot on time interval $t \in [t_{k-1}, t_k]$ with $\alpha(t) = \alpha^k$ and with constant $\dot{n}_w(t)$ is called k-th *path segment*. In particular, if $\dot{n}_w(t) > 0$, it is a *forward path segment*, otherwise if $\dot{n}_w(t) < 0$ it is a *backward path segment*. On each segment, the linear and angular velocities are constant, i.e. $v_{lp}(t) = v_{lp}^k$ and $\omega_{lp}(t) = \omega_{lp}^k$ on interval $t \in [t_{k-1}, t_k]$. Moreover, the constant curvature radius r_{lp}^k is constant and depends only on steering angle α^k,

$$r_{lp}^k = \frac{v_{lp}^k}{\omega_{lp}^k} = \frac{L}{\tan(\alpha^k + \alpha_{off})} \tag{7}$$

The expression of orientation increment is computed as

$$
\begin{aligned}
r_\theta^k =& q_\theta(t_k) - q_\theta(t_{k-1}) = \int_{t_{k-1}}^{t_k} \dot{q}_\theta(\tau)\ d\tau \\
=& \frac{s_w \cos\alpha_{off}}{L} \int_{t_{k-1}}^{t_k} \dot{n}_w(\tau) \sin\alpha(\tau)\ d\tau + \frac{s_w \sin\alpha_{off}}{L} \int_{t_{k-1}}^{t_k} \dot{n}_w(\tau) \cos\alpha(\tau)\ d\tau
\end{aligned} \tag{8}
$$

If the steering angle $\alpha(t) = \alpha^k$ is constant in time interval $[t_{k-1}, t_k]$, then $\sin\alpha^k$ and $\cos\alpha^k$ can be exported from the above integrals. The quantities $n_w^k = \int_{t_{k-1}}^{t_k} \dot{n}_w(\tau) d\tau$ and $\alpha = \alpha^k$ can be measured by the encoders of the robot. Thus, the analytical expression of angular increment is

$$
r_\theta^k = (n_w^k \sin\alpha^k)\ \frac{s_w \cos\alpha_{off}}{L} + (n_w^k \cos\alpha^k)\ \frac{s_w \sin\alpha_{off}}{L} \tag{9}
$$

The control variables n_w^k and α^k have been deliberately separated from the unknown calibration parameters s_w and α_{off} since they can be measured by the robot encoders on actuated wheels and on the steer axis. The integration of position components is simplified on a given segment. In particular, the curvature radius is constant and $q_\theta(t) = q_\theta(t_{k-1}) + \omega_{lp}^k (t - t_{k-1})$. The relative robot motion $r_{pos}^k = [r_x, r_y]^\top$ is obtained by integrating the position component of eq. (1) on a segment.

$$
\begin{aligned}
r_{pos}^k &= \mathrm{R}\left(-q_\theta(t_{k-1})\right) \left(q_{pos}(t_k) - q_{pos}(t_{k-1})\right) \\
&= \int_{t_{k-1}}^{t_k} v_{lp}^k \begin{bmatrix} \cos\left(\omega_{lp}^k(\tau - t_{k-1})\right) \\ \sin\left(\omega_{lp}^k(\tau - t_{k-1})\right) \end{bmatrix} d\tau \\
&= \int_0^{r_\theta^k} \frac{v_{lp}^k}{\omega_{lp}^k} \begin{bmatrix} \cos(\gamma) \\ \sin(\gamma) \end{bmatrix} d\gamma = \frac{L}{\tan(\alpha^k + \alpha_{off})} \begin{bmatrix} \sin r_\theta^k \\ 1 - \cos r_\theta^k \end{bmatrix}
\end{aligned} \tag{10}
$$

where the integration variable τ has been substituted by $\gamma = \omega_{lp}^k(\tau - t_{k-1})$. Equations (9) and (10) give the value of relative robot motion on time interval $[t_{k-1}, t_k]$ under the assumption that the input controls are constant over the interval. Intrinsic calibration can be achieved by keeping constant input controls for specific time intervals.

Althohugh the value of r^k_{pos} cannot be easily measured, the relative orientation r^k_θ is equal to the relative sensor orientation s^k_θ on $[t_{k-1}, t_k]$. Thus, all the terms of equation (9) can be measured by internal or external sensors. All the unknown variables in such equation can be collected into the vector

$$\psi = \begin{bmatrix} \psi_1 \\ \psi_2 \end{bmatrix} = \frac{1}{L} \begin{bmatrix} s_w \cos \alpha_{off} \\ s_w \sin \alpha_{off} \end{bmatrix} \tag{11}$$

Given the measured values of n^k_w, α^k and s^k for several path segments $[t_{k-1}, t_k]$ with $k = 1, \ldots, n$, a linear system $A_\psi \psi = b_\psi$ is defined by n instances of equation (9) with the matrix and known term vector

$$A_\psi = \begin{bmatrix} n^1_w \sin \alpha^1 & n^1_w \cos \alpha^1 \\ \vdots & \vdots \\ n^n_w \sin \alpha^n & n^n_w \cos \alpha^n \end{bmatrix}, \quad b_\psi = \begin{bmatrix} s^1_\theta \\ \vdots \\ s^n_\theta \end{bmatrix} \tag{12}$$

If there are more than two independent equations, the linear system is overdetermined. Hence, the value of ψ that better meets the given conditions is the one that minimizes the error, i.e.

$$\psi^* = \underset{\psi}{\operatorname{argmin}} \, \| A_\psi \psi - b_\psi \|^2 \tag{13}$$

Such problem can be solved by computing the Moore–Penrose pseudoinverse of matrix A_ψ

$$\psi^* = (A^\top_\psi A_\psi)^{-1} A^\top_\psi b_\psi \tag{14}$$

The existence of the pseudoinverse of A_ψ is discussed in detail in section 5.1. Given the value of ψ, the corresponding intrinsic parameters are estimated from equation (11) as

$$\alpha_{off} = \operatorname{atan2}(\psi^*_2, \psi^*_1) \tag{15}$$

$$s_w = L \sqrt{{\psi^*}^2_1 + {\psi^*}^2_2} \tag{16}$$

Since the wheelbase $L > 0$ is known by hypothesis, equations (15) and (16) provide the desired values of the two intrinsic parameters.

4.2. Asymmetric Intrinsic Calibration

The ATC problem in Definition 3.2 is an extension of the STC problem illustrated in the previous section. After the substitution of α_{off} with α_F

and α_B depending on the motion direction, the equations (9) and (10) still hold. Let the path segments be sorted so that the first $\bar{n} < n$ segments are acquired during forward robot motion and the remaining ones during backward motion: $n_w^k \geqslant 0$ for all $k = 1, \ldots, \bar{n}$ and $n_w^k < 0$ for $k = \bar{n}+1, \ldots n$. The orientation equations (9) for each k-th segment are then split into two groups according to the direction. Following the same procedure, a different unknown vector ψ of 4 variables is defined as

$$\psi = \left[\begin{array}{c} \psi_F \\ \hline \psi_B \end{array}\right] = \left[\begin{array}{c} \psi_1 \\ \psi_2 \\ \hline \psi_3 \\ \psi_4 \end{array}\right] = \frac{1}{L} \left[\begin{array}{c} s_w \cos\alpha_F \\ s_w \sin\alpha_F \\ \hline s_w \cos\alpha_B \\ s_w \sin\alpha_B \end{array}\right] \tag{17}$$

The orientation equations are arranged into a linear system with matrix and known term vector

$$\begin{aligned} A_\psi &= \left[\begin{array}{c|c} A_{\psi,F} & 0 \\ \hline 0 & A_{\psi,B} \end{array}\right] \\ &= \left[\begin{array}{cc|cc} n_w^1 \,\mathrm{s}\,\alpha^1 & n_w^1 \,\mathrm{c}\,\alpha^1 & 0 & 0 \\ \vdots & \vdots & \vdots & \vdots \\ n_w^{\bar{n}} \,\mathrm{s}\,\alpha^{\bar{n}} & n_w^{\bar{n}} \,\mathrm{c}\,\alpha^{\bar{n}} & 0 & 0 \\ \hline 0 & 0 & n_w^{\bar{n}+1} \,\mathrm{s}\,\alpha^{\bar{n}+1} & n_w^{\bar{n}+1} \,\mathrm{c}\,\alpha^{\bar{n}+1} \\ \vdots & \vdots & \vdots & \vdots \\ 0 & 0 & n_w^n \,\mathrm{s}\,\alpha^n & n_w^n \,\mathrm{c}\,\alpha^n \end{array}\right] \end{aligned} \tag{18}$$

$$b_\psi = \left[\begin{array}{cccc|ccc} s_\theta^1 & \ldots & s_\theta^{\bar{n}} & & s_\theta^{\bar{n}+1} & \ldots & s_\theta^n \end{array}\right]^\top \tag{19}$$

where the symbols $\mathrm{c}\,\alpha^k = \cos\alpha^k$ and $\mathrm{s}\,\alpha^k = \sin\alpha^k$ have been introduced for brevity. Thus, the intrinsic parameters for ATC problem can be solved by minimizing $\|A_\psi \psi - b_\psi\|$ subject to the condition $\psi_F^\top \psi_F = \psi_B^\top \psi_B$. This consistency constraint is quadratic and comes from the observation that the driving scale s_w is the same in both forward and backward motions. The goal function and constraints can be written as explicit quadratic functions

$$\begin{aligned} \min \;& \tfrac{1}{2}\psi^\top M_\psi \psi - P_\psi^\top \psi + \tfrac{1}{2} b_\psi^\top b_\psi \\ \text{s.t.} \;& \psi^\top W_\psi \psi = 0 \end{aligned} \tag{20}$$

where the matrices M_ψ, P_ψ and W_ψ have the following explicit expressions

$$M_\psi = A_\psi^\top A_\psi = \left[\begin{array}{cc|cc} m_1 & m_2 & 0 & 0 \\ m_2 & m_3 & 0 & 0 \\ \hline 0 & 0 & m_4 & m_5 \\ 0 & 0 & m_5 & m_6 \end{array}\right] \tag{21}$$

$$P_\psi = A_\psi^\top b_\psi = \left[\begin{array}{cccc} p_1 & p_2 & p_3 & p_4 \end{array}\right]^\top \tag{22}$$

$$W_\psi = \left[\begin{array}{c|c} I_2 & 0 \\ \hline 0 & -I_2 \end{array}\right] = \left[\begin{array}{cc|cc} w_1 & 0 & 0 & 0 \\ 0 & w_2 & 0 & 0 \\ \hline 0 & 0 & w_3 & 0 \\ 0 & 0 & 0 & w_4 \end{array}\right] \tag{23}$$

where $w_1 = w_2 = 1$ and $w_3 = w_4 = -1$. Problem (20) is a quadratic programming problem subject to a quadratic equality constraint (QPQEC) [31]. The feasibility of such problem and the uniqueness of its solution depend on the properties of matrices W_ψ and M_ψ. Matrix W_ψ is always full rank. M_ψ is positive semi-definite by construction whereas the conditions for its being positive definite will be given in section 5. Its solution requires a change of variables $\xi = S_c V^\top \psi$ to diagonalize matrix M_ψ, where

$$V = \left[\begin{array}{cc} \mathrm{R}\left(\frac{\mathrm{atan2}(-2m_2, m_3 - m_1)}{2}\right) & 0 \\ 0 & \mathrm{R}\left(\frac{\mathrm{atan2}(-2m_5, m_6 - m_4)}{2}\right) \end{array}\right]$$

and S_c is a diagonal matrix whose diagonal elements are $s_{c,i} \in \{-1, 1\}$ with $i = 1, \ldots, 4$ (hence, $S_c^\top = S_c^{-1} = S_c$). Each $s_{c,i}$ is chosen such that all the elements c_i of vector $c = S_c V P_\psi$ have a non-positive value, i.e. $c_i \leqslant 0$. Hence, it is sufficient to compute VP_ψ and to set $s_{c,i} = -1$ for the positive elements of VP_ψ, otherwise $s_{c,i} = 1$. After the change of variables, we obtain a problem equivalent to (20) with form

$$\begin{array}{ll} \min & \frac{1}{2}\sum_{i=1}^4 d_i \xi_i^2 + \sum_{i=1}^4 c_i \xi_i \\ \text{s.t.} & \sum_{i=1}^4 w_i \xi_i^2 = 0 \end{array} \tag{24}$$

where d_i are the non-negative elements of diagonal matrix $V^\top S_c^\top M_\psi S_c V$ (M_ψ is positive semi-definite), and c_i are the elements of vector $c = S_c V P_\psi$. The matrix W_ψ is invariant to the change of variables since $S_c V^\top W_\psi V S_c = W_\psi$.

Proposition 4.1. *If $c_i \leqslant 0$ for each i, then there exists an optimal solution $\xi^* = [\xi_1^*, \ldots, \xi_4^*]^\top$ of (24) with $\xi_i^* \geqslant 0$ for each i.*

Proof. Suppose that the optimal solution of (24) is s.t. $\xi_i^* < 0$ for some i. Then, the value of objective function, after changing ξ_i^* with $-\xi_i^*$, is less or equal than such supposed optimal solution, since $c_i \leqslant 0$ (strictly less if $c_i < 0$). □

Being a QPQEC, the Karush-Kuhn-Tucker (KKT) conditions hold and the Lagrangian associated to (24) can be defined with the multiplier λ for the equality constraint. The critical points of the Lagrangian function satisfy for $i = 1, \ldots, 4$ the conditions

$$\begin{aligned} d_i\xi_i + c_i + \lambda w_i \xi_i &= 0 \\ \xi_i = -\frac{c_i}{d_i + \lambda w_i} &\geqslant 0 \end{aligned} \tag{25}$$

where the inequality in (25) follows from optimality condition of Proposition 4.1. The inequality is satisfied when the Lagrange multiplier λ lies in the interval (A, B) defined as

$$A = \max_{i\,:\,w_i>0} \left\{ -\frac{d_i}{w_i} \right\} < \lambda < \min_{i\,:\,w_i<0} \left\{ -\frac{d_i}{w_i} \right\} = B \tag{26}$$

Observe that if both $A = B = 0$ (when M_ψ is not positive definite) the interval is empty. The expression of ξ_i in equation (25) can be substituted into the equality constraint of (24) yielding

$$g(\lambda) = \frac{1}{2} \sum_{i=1}^{4} w_i \left(\frac{c_i}{d_i + \lambda w_i} \right)^2 = 0$$

The derivative $g'(\lambda)$ is negative for $\lambda \in (A, B)$. Besides,

$$\lim_{\lambda \to A^+} g(\lambda) = +\infty, \quad \lim_{\lambda \to B^-} g(\lambda) = -\infty$$

Thus, there exists a unique λ^* such that $g(\lambda^*) = 0$ on interval (A, B) and can be straightforwardly found using any numerical technique for algebraic equations like bisection or Newton–Raphson methods. The back-substitution of λ^* into equation (25) allows us to find ξ^* and, recursively, ψ^*. Finally, the asymmetric intrinsic parameters are found as

$$\alpha_F = \operatorname{atan2}\left(\psi_2^*, \psi_1^*\right), \quad \alpha_B = \operatorname{atan2}\left(\psi_3^*, \psi_4^*\right) \tag{27}$$

$$s_w = L\sqrt{{\psi^*}_1^2 + {\psi^*}_2^2} = L\sqrt{{\psi^*}_3^2 + {\psi^*}_4^2} \tag{28}$$

Since there are two equations for s_w, in practice it is computed as the average of the two estimations to balance the potential (and very slight) floating-point arithmetic errors.

4.3. Extrinsic Calibration

The aim of extrinsic calibration is to compute the pose of the sensor mounted on the robot represented by pose $l \in \mathrm{se}(2)$. The value of l is obtained from the comparison between the sensor egomotion measurements s^k over different path segments defined in section 3 and the robot motion r^k measured from odometry. Once the intrinsic calibration is solved, r^k can be computed using the intrinsic parameters and equation (9). Equation (5) describes the spatial relationship between these poses and can be expanded into position and angular parts as

$$\begin{bmatrix} l_{pos} + \mathrm{R}\left(l_\theta\right) s^k_{pos} \\ l_\theta + s^k_\theta \end{bmatrix} = \begin{bmatrix} r^k_{pos} + \mathrm{R}\left(r^k_\theta\right) l_{pos} \\ r^k_\theta + l_\theta \end{bmatrix} \tag{29}$$

where the subscript $\cdot_{pos}$ refers to the position coordinate vector of a pose. The angular part of equation (29) has been already used to substitute $r^k_\theta = s^k_\theta$ in equation (8) to solve the STC and ATC problems. The position part of equation (29) enables us to estimate the value of extrinsic parameters l. In particular, the position error on k-th measurement can be defined as

$$\begin{aligned} e^k_{pos} &= (l \oplus s^k)_{pos} - (r^k \oplus l)_{pos} \\ &= \left(l_{pos} + \mathrm{R}\left(l_\theta\right) s^k_{pos}\right) - \left(r^k_{pos} + \mathrm{R}\left(r^k_\theta\right) l_{pos}\right) \\ &= \underbrace{\begin{bmatrix} I_2 - \mathrm{R}\left(r^k_\theta\right) & \mathrm{R}\left(s^k_{pos}\right) \end{bmatrix}}_{Q_k} \underbrace{\begin{bmatrix} \varphi_{pos} \\ \varphi_{ang} \end{bmatrix}}_{\varphi} - r^k_{pos} \end{aligned} \tag{30}$$

where $\varphi_{pos} = [\varphi_1, \varphi_2]^\top = [l_x, l_y]^\top$ and $\varphi_{ang} = [\varphi_3, \varphi_4]^\top = [\cos l_\theta, \sin l_\theta]^\top$. The vector φ_{ang} is subject to constraint $\varphi^\top_{ang}\varphi_{ang} = 1$ to satisfy trigonometric consistency that can be written as

$$\begin{aligned} h(\varphi) = \varphi_3^2 + \varphi_4^2 - 1 &= \varphi^\top \begin{bmatrix} 0 & 0 \\ 0 & I_2 \end{bmatrix} \varphi - 1 \\ &= \varphi^\top\, W\, \varphi - 1 = 0 \end{aligned} \tag{31}$$

The error function can be chosen in order both to properly represent a distance from the consistent estimation and to allow the computation of its

minimum. Such function must depend on all the measurements collected by the robot, while moving along the n path segments. Although more complex functions could weigh the different components of e^k_{pos}, it is convenient to use the square sum function defined as

$$\begin{aligned} E(\varphi) &= \sum_{k=1}^{n} {e^k_{pos}}^\top e^k_{pos} \\ &= \sum_{k=1}^{n} (\varphi^\top Q_k - {r^k}_{pos})^\top (Q_k\ \varphi - r^k_{pos}) \\ &= \varphi^\top M_\varphi \varphi - 2\varphi^\top P_\varphi + \left(\sum_{k=1}^{n} {r^k_{pos}}^\top\ r^k_{pos} \right) \end{aligned} \tag{32}$$

where

$$M_\varphi = \sum_{k=1}^{n} Q_k^\top\ Q_k = \begin{bmatrix} m_1 & 0 & m_2 & -m_3 \\ 0 & m_1 & m_3 & m_2 \\ m_2 & m_3 & m_4 & 0 \\ -m_3 & m_2 & 0 & m_4 \end{bmatrix} \tag{33}$$

$$m_1 = \sum_{k=1}^{n} 2(1 - \cos r^k_\theta) \tag{34}$$

$$m_2 = \sum_{k=1}^{n} \left(s^k_x\ (1 - \cos r^k_\theta) - s^k_y\ \sin r^k_\theta \right) \tag{35}$$

$$m_3 = \sum_{k=1}^{n} \left(s^k_x\ \sin r^k_\theta + s^k_y\ (1 - \cos r^k_\theta) \right) \tag{36}$$

$$m_4 = \sum_{k=1}^{n} \left((s^k_x)^2 + (s^k_y)^2 \right) \tag{37}$$

$$\begin{aligned} P_\varphi &= \sum_{k=1}^{n} Q_k^\top\ r^k_{pos} = \sum_{k=1}^{n} \begin{bmatrix} (I_2 - R^\top(r^k_\theta))\ r^k_{pos} \\ R^\top(s^k_{pos})\ r^k_{pos} \end{bmatrix} \\ &= \begin{bmatrix} p_1 & p_2 & p_3 & p_4 \end{bmatrix}^\top \end{aligned} \tag{38}$$

Thus, the extrinsic calibration problem is equivalent to the constrained optimization problem with target function in equation (32) and constraint from equation (31), i.e. to

$$\begin{aligned} \min \quad & E(\varphi) = \varphi^\top M_\varphi \varphi - 2\varphi^\top P_\varphi + \text{const} \\ \text{s.t.} \quad & h(\varphi) = \varphi^\top W_\varphi \varphi - 1 = 0 \end{aligned} \tag{39}$$

There are two values of φ satisfying the above problem as discussed in section 5.1. Therefore, an additional constraint is added to select only one of two valid solutions as suggested in [1], for example $\varphi_1 \geqslant 0$ due to the frontal placement of the sensor. Since $\varphi_1 \geqslant 0$ is an inequality constraint, the KKT conditions must hold thanks to Slater's conditions. The Lagrangian point can be found by solving the linear system $(M_\varphi - \lambda W)\varphi = P$ under the constraint $h(\varphi)$. The system matrix can be decomposed as $(M_\varphi - \lambda W) = L_\varphi D_\varphi L_\varphi^\top$ according to the modified Cholesky decomposition with lower triangular and diagonal matrices

$$L_\varphi = \begin{bmatrix} I_2 & 0 \\ \frac{1}{m_1}\mathrm{R}\left([m_2, -m_3]\right) & I_2 \end{bmatrix},\ D_\varphi = \begin{bmatrix} \mu_1 I_2 & 0 \\ 0 & (\mu_2 - \lambda) I_2 \end{bmatrix}$$

where $\mu_1 = m_1$ and $\mu_2 = (m_1 m_4 - m_2^2 - m_3^2)/m_1$ are the eigenvalues of matrix M_φ (both with multiplicity 2). The expression of φ_3 and φ_4 can be obtained by solving the linear system with the unknown Lagrange multiplier λ and substituted into the constraint. The result of the substitution is the following second-degree polynomial whose solution gives the admissible values of Lagrange multiplier λ

$$\lambda^2 + b_\varphi \lambda + c_\varphi = 0 \tag{40}$$

where its coefficients are

$$\begin{aligned} b_\varphi &= 2\mu_2 \\ c_\varphi &= \mu_2^2 - \frac{(m_1 p_3 - m_2 p_1 - m_3 p_2)^2 + (m_1 p_4 + m_3 p_1 - m_2 p_2)^2}{m_1^2} \end{aligned}$$

Each $\lambda_{1,2}$ satisfying equation (40) can be back-substituted into the linear system and the two respective solutions $\varphi^{(1,2)}$ can be obtained. The existence of two solutions is due to the symmetries of the tricycle model equations. The previously discussed condition $\varphi_1 \geqslant 0$ allows the choice between the two outputs. Section 5 will provide additional insights into the nature of the solution.

5. Formal Discussion of Results

In this section, the formal issues of the calibration algorithm presented in section 4 are discussed.

5.1. Observability

Real AGVs have a unique set of calibration parameters for both STC and ATC problems. The algorithms proposed in the previous section estimate these parameters by finding the values that better match the given input controls and sensor observations. Thus, the calibration procedure is reduced to a set of constrained optimization problems. A formal analysis is required to assess the conditions guaranteeing the existence and uniqueness of the solution both to check the correctness of the proposed methods and, from a practical point of view, to correctly choose the robot motion.

The internal state of a system is observable if its estimation from the input controls and sensor observations is feasible. There are several ways to ascertain the observability of a system as defined from system theory. In the context of tricyle robot calibration, the internal state consists of the intrinsic and extrinsic parameters which do not evolve in time. The method shown in section 4 consists of several equations that return the calibration parameters from the sensor measurements. Here, observability is constructively proved by setting the conditions on the input controls (the trajectories) such that those equations have a unique solution.

The solution of intrinsic calibration, in equations (13) and (20) respectively for STC and ATC formulations, and extrinsic calibration in equation (39) have the form of least-square optimization on quadratic functions. These quadratic functions are equal to the square of overdetermined linear equations representing the relationship between the measurements and the calibration variables. In the case of asymmetric intrinsic and extrinsic calibration, the variables of these linear equations are subject to additional consistency constraints. In the following, the observability of each set of calibration parameters is proven by showing that, under proper conditions, there is a unique solution to the optimization problem.

The estimation of intrinsic parameters for the standard tricycle model has the form of an overdetermined linear system, which is the argument of equation (13). The solution is defined by the pseudoinverse. A condition for the estimation of α_{off} and s_w, i.e. the observability of the two parameters, is given by the following proposition.

Proposition 5.1. *The solution of equation (13) exists and is unique iff the input dataset contains at least two trajectories k_1 and k_2, $k_1 \neq k_2$, s.t. the corresponding steering angles $\alpha^{k_1} \neq \alpha^{k_2} + i\pi$ for some i and $n_w^{k_1}, n_w^{k_2} \neq 0$.*

Proof. If. The solution of (13) exists if the left pseudoinverse of A_ψ in equation (14) exists. The pseudoinverse of a $n \times 2$ matrix exists if A_ψ is full rank, i.e. its rank is 2 in this case. The submatrix obtained from rows k_1 and k_2 has determinant

$$\det \begin{bmatrix} n_w^{k_1} \sin \alpha^{k_1} & n_w^{k_1} \cos \alpha^{k_1} \\ n_w^{k_2} \sin \alpha^{k_2} & n_w^{k_2} \cos \alpha^{k_2} \end{bmatrix} = n_w^{k_1} n_w^{k_2} \sin\left(\alpha^{k_1} - \alpha^{k_2}\right)$$

which cannot be zero due to the hypotheses.
Only if. Let the quadratic function of equation (13) have a unique minimum ψ^*, i.e. ψ^* is a critical point, $A_\psi^\top (A_\psi \psi^* - b_\psi) = 0$, and the Hessian matrix $A_\psi^\top A_\psi$ is positive definite. If $\alpha^{k_1} - \alpha^{k_2} = i\pi$ or $n_w^k = 0$ for all k, k_1, k_2, then $\det(A_\psi^\top A_\psi) = 0$ contradicting $A_\psi^\top A_\psi$ positive definiteness. □

The observability proof for intrinsic ATC and extrinsic parameters follows a similar pattern with the difference that there are other constraints on the variables. In section 4.2, the method for estimating the asymmetric intrinsic parameters has been illustrated and the discussion has shown that there is a unique global solution. The following proposition explicitly states the conditions for which this result holds.

Proposition 5.2. *Let $\alpha^{k_1} \neq \alpha^{k_2} + i\pi$ and $n_w^{k_1}, n_w^{k_2} \neq 0$ for at least two forward segments $0 < k_1 < k_2 \leqslant \bar{n}$, $\alpha^{k_3} \neq \alpha^{k_4} + j\pi$ and $n_w^{k_3}, n_w^{k_4} \neq 0$ for at least two backward path segments $\bar{n} < k_3 < k_4 \leqslant n$. Then, the problem (20) is feasible and its solution is unique.*

Proof. The discussion of calibration method in section 4.2 shows the existence and uniqueness of the solution according to [31], assuming that M_ψ is positive definite. The hypotheses on forward and backward path segments are sufficient to prove the positive definiteness of M_ψ, similarly to the proof of Proposition 5.1. □

Propositions 5.1 and 5.2 also provide criteria to correctly choose the minimum number of path segments and the steering angles.

It remains to be discussed the feasibility of extrinsic calibration, which is common between STC and ATC formulation. The first issue concerns the number of solutions of the extrinsic calibration problem. Under the conditions discussed in the following, there are two symmetric solutions $l = [l_x, l_y, l_\theta]^\top$ and $l' = [-l_x, -l_y, l_\theta + \pi]^\top$. However, the additional constraint due to the physical placement of the sensor allows their disambiguation.

The second critical issue is related to the existence of only two solutions. Although the extrinsic calibration is a QPQEC, it cannot be solved using the same procedure of intrinsic ATC due to the rank of quadratic constraint matrix W. The procedure in section 4.3 leads to a closed-form solution by solving a parametric linear system. The solution of such system depends on the positive definiteness of matrix M_φ, which is always at least semi-positive definite. The following proposition gives the additional conditions on the robot paths granting the feasibility of the problem.

Proposition 5.3. *Let $n > 1$, $r_\theta^{k_1} \neq 2\pi i$ and $\|s_{pos}^{k_2}\| > 0$ for some $0 < k_1, k_2 \leq n$ and $i \in \mathbb{Z}$. Then, the problem (39) is feasible and has two solutions.*

Proof. Observe that all the terms of the sum in equations (34) and (37) are non-negative and $m_1, m_4 \geq 0$. Hence, if there is at least one $r_\theta^{k_1} \neq 2\pi i$, then $\cos r_\theta^{k_1} < 1$ and $m_1 > 0$. Similarly, if there is $\|s_{pos}^{k_2}\| > 0$, then also $m_4 > 0$. The eigenvalues of M_φ are m_1 and $(m_1 m_4 - m_2^2 - m_3^2)/m_1$, both with multiplicity 2. Using triangular and Cauchy-Schwartz inequalities, it is straightforward to show that

$$m_1 m_4 \geqslant 2 \sum_{k=1}^{n} (1 - \cos s_\theta^k) \|s_{pos}^k\| \geqslant m_2^2 + m_3^2 \tag{41}$$

When the hypotheses are all satified, the strict inequality holds, the eigenvalues are all positive and M_φ is positive definite. □

5.2. Error Propagation

Numerical robustness is an important property to be considered in order to successfully apply the proposed technique to real world AGV calibration. However careful the sensor measurements are, the input data of the calibration are invariably noisy and uncertain. There are several ways to assess the numerical robustness of an algorithm. The statistical evaluation of the calibration parameters computed in repeated trials and different conditions is the more direct and effective approach and will be presented in section 6. On the other hand, the numerical analysis of the algorithms allows a consideration of all the possible occurences that cannot be experimentally reproduced and also the identification of all the most convenient conditions. The propagation of error in a procedure can be measured by the variance or by the deterministic error of the computed parameters. Since the calibration parameter equations, such as equations (13), (20) and (39), are linear

or nearly linear, their numerical stability depends on the *condition number* of the problem matrix.

The solution of intrinsic STC requires the solution of an overdetermined linear system where the matrix A_ψ depends on the parameters of the path segment, i.e. the steering angles α^k and the travelled path length n_w^k, and the known term vector b_ψ is a function of sensor angular displacements s_θ^k. Most of uncertainty lies in the egomotion estimation of s_θ^k, but the propagation of uncertainty is affected by condition number $\kappa(A_\psi)$ and, hence, by the choice of path segments. In the general case, the expression of $\kappa(A_\psi)$ cannot be straightforwardly obtained, but the path segments are chosen according to regularity criteria. For example, the AGVs perform paths with the same steering angle both on left and right, i.e. $\alpha^{n-k} = -\alpha^k$ (the order of α^k is not restrictive), and the angular length of all the paths is approximately equal to β, i.e. $n_w^k = \frac{\beta L}{\sin \alpha^k}$. The straight trajectory is not used in the proposed calibration procedure for a practical reason: it is easier to sequentially execute uniform circular paths in a bounded space by progressively increasing the value of steering $|\alpha|$. Although possible, the inclusion of a straight path segment would require a specific and time-consuming positioning of the robot. Hence, in the following the steering angles $|\alpha^k| > 0$ are never null. The minimum $|\alpha|$ corresponds to the maximum radius of path segments. The maximum value of $|\alpha|$ depends on the mechanical limits of the steering wheel.

Proposition 5.4. *Let matrix A_ψ in equation (12) be s.t. $\alpha^{n-k} = -\alpha^k$, $|\alpha^k| > 0$ and $n_w^k = \beta L / \sin \alpha^k$ where $k = 1, \ldots, n$ and β is the angular length of path segments. Then, the condition number of problem in equation (13) is equal to*

$$\kappa(A_\psi) = \frac{\max\left\{n, \sum_{k=1}^n \tan^{-2} \alpha^k\right\}}{\min\left\{n, \sum_{k=1}^n \tan^{-2} \alpha^k\right\}} \tag{42}$$

Proof. The condition number is obtained from the minimum and maximum singular values of A_ψ that can be found by computing $A_\psi^\top A_\psi$. Due to the symmetry hypothesis $\alpha^{n-k} = -\alpha^k$, the non-diagonal terms of $A_\psi^\top A_\psi$ are zero, $(\beta L)^2 \sum_{k=1}^n (1/\tan \alpha^k) = 0$. Thus, $A_\psi^\top A_\psi$ is diagonal with elements $(\beta L)^2 n$ and $(\beta L)^2 \sum_{k=1}^n \tan^{-2} \alpha^k$. The thesis follows from the definition of condition number. □

Given the discussed hypotheses, the problem is well-conditioned if the average value of $|\alpha^k|$ is close to $\pi/4$. A steering angle above 50° stresses the steer mechanics and increases friction and slip between the rubber wheels

and the ground. Thus, a trade-off between well-conditioned data given by relatively large steering angle and motion accuracy must be found.

The same considerations on error propagation extend to the intrinsic ATC problem. Although the asymmetric calibration involves the solution of a constrained linear system, the structure of matrix A_ψ in equation (18) is similar to the standard case. The main difference lies in the separate management of the path segments according to the direction of the AGV motion.

6. Experiments

The proposed calibration algorithm has been implemented and tested on industrial AGVs in warehouse buildings. Two vehicle models have been used in the experiments for data collection and performance analysis: the CB16 and the CB25 (manufactured by Elettric80 S.p.A.), both compliant with the tricycle model illustrated in section 3. The choice of CB16 or CB25 for the experiments discussed in this section is related to the AGV availability in the specific setting, where the experiment is performed. The CB25 is shown in Figure 1. The AGV front with the actuated wheel is at the opposite side of the fork-lift. The robot is equipped with four laser scanners for safety (Sick S3000 and S300) with a scanning plane close to the ground plane, and one laser scanner for navigation (Sick NAV350). The navigation laser scanner allows the detection of artificial reflective markers in the environments that are used as landmarks for localization and egomotion estimation. The reflective markers, which are commonly placed in industrial warehouses, correspond to stable and easily distinguishable points in a laser scan. Thus, the association of corresponding landmarks between two scans is reliable and substantially free of outliers.

The proposed calibration method for STC and ATC models has been implemented on a PLC software system providing a real-time controller. This PLC is programmed using its IEC 61131-3 compatible language. While this language is suitable for control and low-level interface, it lacks comprehensive libraries for numeric computation, linear algebra operations, and data structure operations. However, since the proposed solutions of calibration problems are based on either closed-form formulations or simple numerical algorithms (e.g. bisection technique), their implementation has proven straightforward. The calibration module also handles motion on each forward and backward segment with a specific constant steering angle, acquisition of

n_{seg}	α-min/max [deg]	β [deg]	v_w [mm/s]	α_{off} [cdeg] avg	std	s_w [mm/tick] avg	std	l_x [mm] avg	std	l_y [mm] avg	std	l_θ [cdeg] avg	std
2	18 ÷ 50	180	1000	-75.93	0.39	0.249685	0.000036	390.28	0.13	2.14	0.14	50.34	0.32
4	18 ÷ 34	180	1000	-75.89	0.30	0.249806	0.000023	389.09	0.16	1.63	0.27	43.03	0.21
4	18 ÷ 50	60	1000	-77.05	0.72	0.249576	0.000043	395.79	0.34	4.21	0.63	36.88	1.18
4	18 ÷ 50	120	1000	-75.36	0.32	0.249880	0.000059	386.68	0.51	6.17	0.22	37.83	0.70
4	18 ÷ 50	180	800	-76.73	0.59	0.249652	0.000111	387.81	0.60	2.78	0.18	44.57	0.28
4	18 ÷ 50	180	1000	-76.27	0.62	0.249668	0.000040	387.10	0.25	2.48	0.47	44.64	0.80
4	18 ÷ 50	180	1200	-75.82	0.35	0.249690	0.000007	387.89	0.66	1.85	0.22	47.30	1.12
4	18 ÷ 50	180	1400	-75.57	0.63	0.249686	0.000023	388.04	0.43	1.81	0.15	48.19	0.77
4	35 ÷ 50	180	1000	-73.69	0.44	0.250081	0.000004	386.03	0.22	0.00	0.26	43.01	1.80
6	18 ÷ 50	180	1000	-76.01	0.31	0.249816	0.000085	389.03	0.32	1.82	0.53	43.35	0.44
8	18 ÷ 50	180	1000	-75.64	0.11	0.249750	0.000015	389.23	0.09	2.79	0.28	40.46	0.59
10	18 ÷ 50	180	1000	-75.03	0.09	0.249772	0.000023	388.94	0.17	3.23	0.12	42.65	0.34
4	18 ÷ 34	180	800	-77.47	0.48	0.249716	0.000122	389.00	0.03	2.03	0.48	41.84	1.73
4	18 ÷ 34	180	1200	-77.74	0.30	0.249789	0.000006	388.91	0.39	1.73	0.12	42.10	0.50
4	18 ÷ 34	180	1400	-77.40	0.65	0.249736	0.000039	389.45	0.37	1.97	0.56	42.26	0.54
6	18 ÷ 34	180	800	-75.48	0.33	0.249731	0.000061	389.48	0.15	2.47	0.24	41.24	0.28
6	18 ÷ 34	180	1000	-75.75	0.29	0.249753	0.000027	389.29	0.45	2.52	0.41	40.38	0.79
6	18 ÷ 34	180	1200	-74.74	0.16	0.249706	0.000027	389.76	0.45	2.50	0.49	41.84	0.47
6	18 ÷ 34	240	1200	-75.03	0.11	0.249807	0.000007	390.13	0.15	4.49	0.38	38.08	0.35
6	18 ÷ 50	240	800	-75.49	0.16	0.249744	0.000052	390.14	0.21	6.77	0.35	39.58	0.55

Table 1: Standard Tricycle Calibration parameters at different conditions for a CB16 AGV

measurements from encoders and laser scanners, and registration of artificial landmarks.

The robot egomotion is estimated exploiting the landmarks detected by the navigation range finder. The landmarks observed from different scans are associated and aligned using a registration algorithm similar to [32, 33]. Theoretically, it should be sufficient to compare the landmark sets at the beginning and the end of the trajectory in order to compute the AGV motion along a segment. In practice, this operation is repeated for each pair of consecutive scans to track landmark associations and to avoid data association errors. Markers are matched according to the nearest neighbor criterion. When the landmark map is available, it can be used to further attenuate the uncertainty associated with sensor measurements. Moreover, the AGV is not moving during the acquisition of the initial and final landmark sets to avoid position errors on the detected landmarks due to the robot motion. Registration with landmarks is much more robust and accurate than generic scan matching methods such as [1] and substantially free of outliers.

The proposed calibration methods for STC and ATC require forward and backward robot motions along circular path segments as illustrated in section 4. In the specific case of ATC, the forward and backward motions are treated separately to compute the forward and backward steer offsets. Moreover, the AGV follows trajectories with different steering values and directions, i.e. left and right steering angles (respectively positive and negative). The setup required for AGV calibration is a free area in the warehouse large enough to accommodate circular trajectories with maximum radius of

n_{seg}	α-min/max	β	v_w	α_F [cdeg]		α_B [cdeg]		s_w [mm/tick]		l_x [mm]		l_y [mm]		l_θ [cdeg]	
	[deg]	[deg]	[mm/s]	avg	std	avg	std	avg	std	avg	std	avg	std	avg	std
2	18 ÷ 50	180	1000	-74.84	0.81	-77.13	0.33	0.249746	0.000038	390.27	0.16	2.21	0.10	50.32	0.40
4	18 ÷ 34	180	1000	-72.30	0.43	-79.22	0.47	0.249888	0.000008	389.09	0.20	1.43	0.36	42.98	0.26
4	18 ÷ 50	60	1000	-71.59	0.76	-82.81	0.52	0.249664	0.000029	395.79	0.42	4.34	0.50	36.82	1.46
4	18 ÷ 50	120	1000	-73.24	0.07	-76.00	0.62	0.249978	0.000040	386.68	0.63	5.33	0.19	37.81	0.85
4	18 ÷ 50	180	800	-75.71	0.61	-76.76	0.82	0.249717	0.000129	387.80	0.73	2.23	0.49	44.56	0.34
4	18 ÷ 50	180	1000	-75.07	1.04	-76.69	0.36	0.249762	0.000047	387.10	0.30	2.04	0.48	44.63	0.98
4	18 ÷ 50	180	1200	-75.09	0.41	-76.28	0.55	0.249790	0.000030	387.89	0.81	1.71	0.68	47.29	1.37
4	18 ÷ 50	180	1400	-74.97	0.99	-75.87	0.39	0.249810	0.000040	388.04	0.52	1.64	0.40	48.18	0.94
4	35 ÷ 50	180	1000	-71.15	0.63	-75.93	0.26	0.250092	0.000005	386.03	0.27	-0.09	0.30	42.96	2.20
6	18 ÷ 50	180	1000	-72.02	0.37	-78.76	0.37	0.249882	0.000105	389.03	0.39	1.16	0.66	43.29	0.53
8	18 ÷ 50	180	1000	-72.70	0.34	-77.47	0.46	0.249823	0.000027	389.23	0.11	2.22	0.39	40.43	0.72
10	18 ÷ 50	180	1000	-71.25	0.44	-77.87	0.39	0.249842	0.000025	388.94	0.21	2.76	0.23	42.60	0.40
4	18 ÷ 34	180	800	-74.79	0.72	-79.68	0.34	0.249776	0.000163	389.00	0.04	1.69	0.66	41.81	2.12
4	18 ÷ 34	180	1200	-74.41	0.39	-80.38	0.34	0.249869	0.000028	388.91	0.48	1.23	0.30	42.06	0.62
4	18 ÷ 34	180	1400	-74.65	0.99	-79.94	0.64	0.249831	0.000034	389.45	0.46	1.82	0.83	42.22	0.66
6	18 ÷ 34	180	800	-72.07	0.48	-78.67	0.34	0.249800	0.000069	389.47	0.18	2.31	0.42	41.19	0.33
6	18 ÷ 34	180	1000	-72.21	0.32	-79.13	0.27	0.249821	0.000028	389.29	0.56	2.40	0.55	40.32	0.96
6	18 ÷ 34	180	1200	-71.42	0.07	-78.05	0.19	0.249788	0.000030	389.77	0.55	2.49	0.56	41.79	0.57
6	18 ÷ 34	240	1200	-72.41	0.23	-78.05	0.34	0.249854	0.000013	390.14	0.18	4.78	0.39	38.04	0.42
6	18 ÷ 50	240	800	-71.74	0.33	-78.40	0.16	0.249791	0.000059	390.14	0.26	6.33	0.51	39.54	0.67

Table 2: Asymmetric Tricycle Calibration parameters at different conditions for a CB16 AGV

5 m.

Two experiments have been designed to assess the correctness and the precision of the proposed calibration method. The goal of the first experiment is the assessment of the six calibration parameters at different calibration conditions. The second experiment estimates the positioning precision of different AGVs at operation points.

6.1. Calibration Condition Experiment

Since the groundtruth parameters are not available, the measurement of the accuracy of the calibration methods can be indirectly performed by assessing the repeatability of the estimation. Therefore, the calibration procedure has been repeated several times using different sets of circular path segments with the AGV moving at different speeds. A CB16 AGV has been calibrated in a warehouse environment with enough space for the required motion. The calibration is organized in four phases each distinguished by the motion direction (forward or backward) and by the steering side (left or right). During each phase, the AGV executes circular path segments and gradually increases the (absolute) value of steering angle α. The curvature radius is equal to $r_{lp} = L/\tan\bar{\alpha}$ at the logical point and $r_w = L/\sin\bar{\alpha}$ at the front wheel. Hence, the radius of circular path segments r_{lp} decreases during a single phase. In order to keep a regular pattern, path segments are circular arcs of fixed angular length β. Hence, the length of a path segment is equal to βr_{lp}, where β is in radians and r_{lp} depends on steering angle α

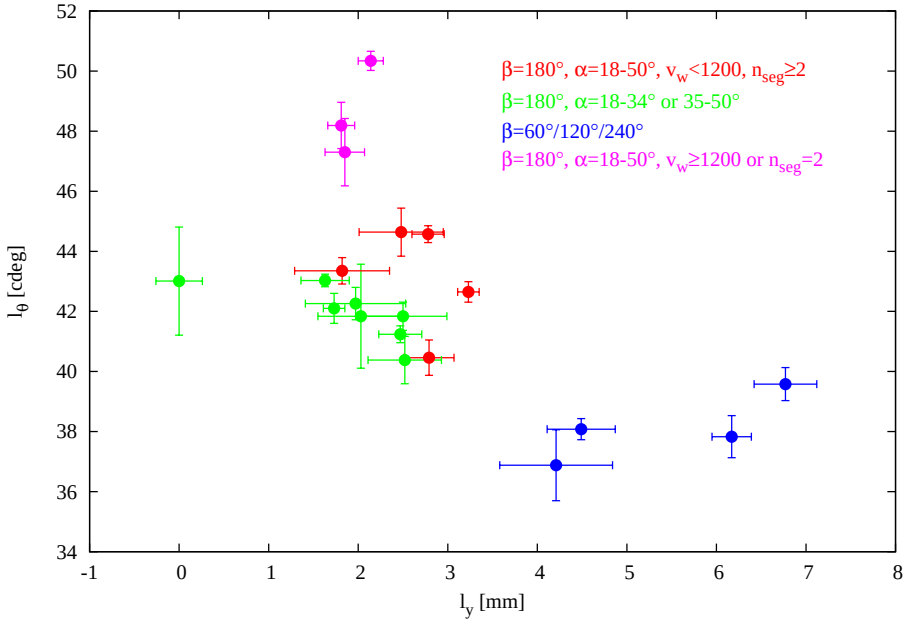

Figure 3: STC calibration parameters l_y and l_θ with standard deviation error bars obtained at different conditions. Color labels highlight values obtained at specific conditions: standard $\beta = 180°$ segment paths, large range of steering angle α and moderate speed (red); $\beta = 180°$ with limited α range (green); $\beta \neq 180°$ segments (blue); standard conditions, but with $n_{seg} = 2$ or higher speed (purple).

as above. For example, if $\beta = \pi$, the robot covers half-circles (henceafter, β is expressed in degrees for reader convenience). In the different trials, we changed the number of path segments n_{seg} used in each phase, the minimum and maximum steering angles α, the angular length of each path segment β, and the speed of the actuated wheel v_w. The complete calibration procedure takes about $8 \div 15$ minutes depending on these parameters and, in particular, on the number of path segments n_{seg}.

The calibration procedure has been performed three or four times for each configuration (n_{seg}, α-min/max, β and v_w) in order to estimate the average value and standard deviation of calibration parameters. Tables 1 and 2 illustrate the results achieved in 63 calibrations for a CB16 AGV according respectively to the STC and ATC models. Given the same calibration setup, the calibration parameters computed according to STC and ATC problems

are very close. The value of the single steer offset α_{off} for STC has an intermediate value between α_F and α_B for ATC. Even with different calibration conditions and with different calibration problems, the computed calibration parameters do not change significantly across the different trials.

The sensor orientation l_θ is the angular parameter that is most sensitive to experimental conditions with differences slight above 10 $cdeg$ (1 $cdeg$ = 0.01°), while l_y is the most sensitive position parameter with differences of about 6 mm (varying from 0.0 to 6.77). The laser scanner cross-sectional coordinate l_y is less steady than the longitudinal one l_x as shown by their respective average value columns. Figure 3 graphically displays the values of l_y and l_θ at different conditions of STC calibration. These two sensitive parameters are more affected by the choice of β, which determines both the length of the path segments and the visible landmarks, by a too low number of segments ($n_{seg} < 4$) or by a high speed during the AGV motion. If a low number of path segments is used (row $n_{seg} = 2$ in Table 2), the standard deviation of α_F is slightly higher and the estimated l_θ is different from the other assessments. The results (in particular, see the values of l_θ in Tables 1 and 2) show that $\beta = 180°$ is the best trade-off that allows sufficiently long trajectories and observation of the landmarks from a similar angle at the beginning and the end of a path segment. In practice, $n_{seg} = 6 \div 8$ has been considered adequate for application purposes and has been adopted in the proposed procedure. With $n_{seg} = 8$ and $\beta = 180°$, complete AGV calibration requires about 12 minutes.

6.2. Position Precision Experiment

Several tasks performed by AGVs require to stop at given points of the warehouse, e.g. to load or unload pallets. The position precision at such operation points depends on different factors including the robot control and navigation system, the pose estimation of the AGV and the calibration parameters. The localization system provides feedback to the control and navigation system in the form of AGV pose w.r.t. an inertial reference frame in the environment. The system computes the motion commands of the AGV in order to reach the operation point. Both the localization and the control-navigation systems exploit the AGV model with the calibration parameters. The intrinsic parameters are part of the robot model and influence both the control system and the prediction of the localizer. The extrinsic parameters define the pose of the navigation laser scanner. An important aim of calibration is to make all the AGVs working in a warehouse stop at the same

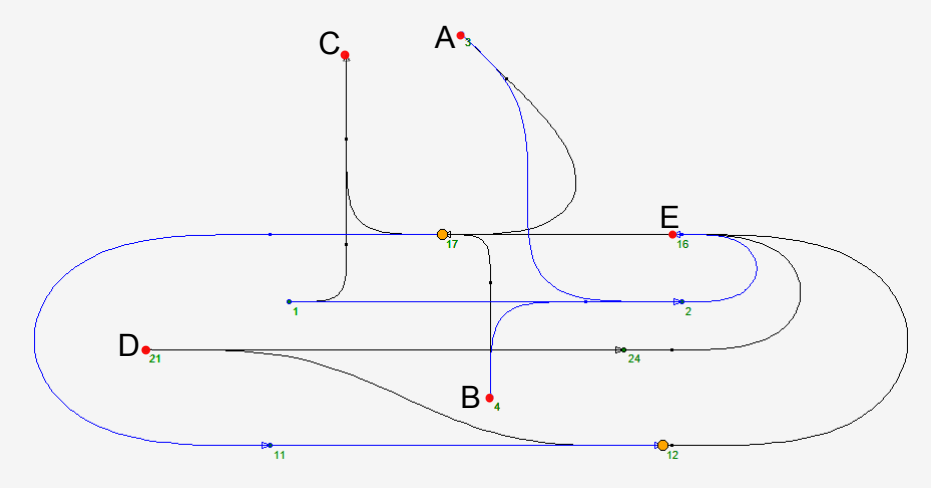

Figure 4: *Setting* 1: trajectory layout and operation points for position precision experiments. Points are labelled with letters A, B, C, D, E. The layout area is approximately 9.3 $m \times 4.2$ m.

operation points with adequate precision.

A set of experiments has been executed in two real warehouses, hereafter termed *Setting* 1 and *Setting* 2, to assess AGV positioning precision obtained by automatic calibration. The CB25 AGVs operating in these two warehouses were available for a limited time for our calibration tests. Hence, we focused on assessing position precision with ATC calibration. In each environment, a set of operation points has been selected. In particular, we have chosen 5 points for *Setting* 1 (labeled with letters A-E) and 10 points for *Setting* 2 (labeled as $P_1 - P_{10}$). Figure 4 shows the path layout of *Setting*

	AGV	α_F [cdeg]	α_B [cdeg]	s_w [mm/tick]	l_x [mm]	l_y [mm]	l_θ [cdeg]
Setting 1	$LGV71^{(a)}$	-88.77	-76.70	0.250911	1485.86	-9.80	236.49
	$LGV74^{(a)}$	-61.68	-56.34	0.249778	1508.43	-9.00	-22.32
	$LGV01^{(a)}$	-87.79	-86.39	0.249122	1500.61	-2.90	-82.36
Setting 2	$R32^{(m)}$	-120.65	-120.65	0.251885	1310	17	140
	$R30^{(a)}$	-107.32	-107.81	0.251801	1293	17	-75
	$R31^{(a)}$	-111.12	124.94	0.252952	1317	7	-131
	$R36^{(a)}$	-107.53	-112.13	0.253143	1294	14	-62

Table 3: Calibration parameters of the AGVs used in *Setting* 1 and *Setting* 2 according to ATC model. Label $^{(a)}$ refers to AGVs calibrated using the proposed method and label $^{(m)}$ to the manually calibrated ones.

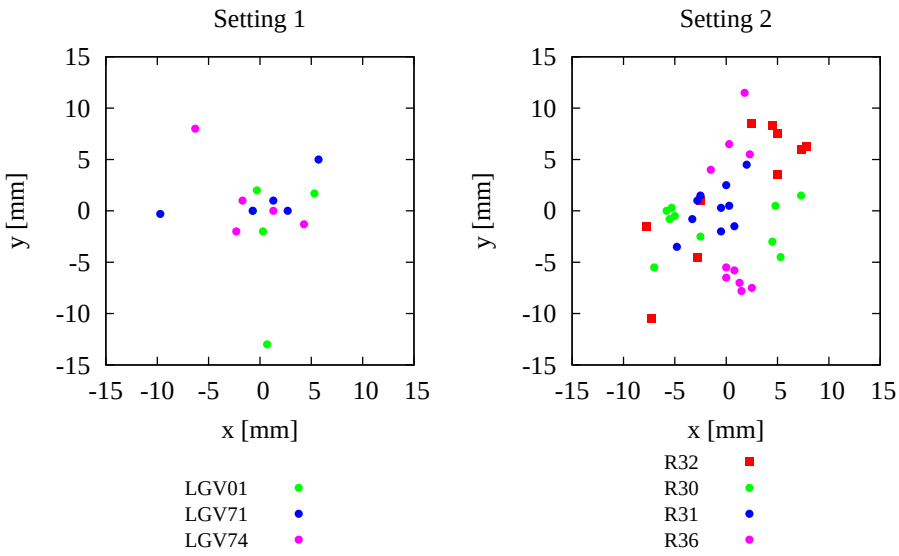

Figure 5: Distribution of halting points around the local reference frames of *Setting* 1 (left) and *Setting* 2 (right). The figure is obtained by overlapping points referred to different local reference frames.

1 with the selected operation points for the purpose of experimentation. Observe that points A and B (purposely defined for this experiment) are reached by uneven and high curvature paths that stress the control system, whereas the other points (C, D and E) are approachable through smoother trajectories. *Setting* 2 refers to an industrial plant with larger size. In this case, the paths to the operation points are compliant with the requirements of a production warehouse and therefore do not include high curvature segments. Paths consist of both straight and curved segments.

The experiments in *Setting* 1 have been performed using three CB25-type AGVs, labelled LGV71, LGV74 and LGV01. In *Setting* 2 four CB25-AGVs, labelled R32, R30, R31 and R36, have been used. All the AGVs are calibrated using the proposed method with ATC model, with the only exception of R32 which has been calibrated according to a manual procedure by an expert operator. The manual procedure has been executed by separately tuning each calibration parameter. The parameter value is iteratively ad-

Operation Points	$LGV71^{(a)}$			$LGV74^{(a)}$			$LGV01^{(a)}$		
	x [mm]	y [mm]	dist [mm]	x [mm]	y [mm]	dist [mm]	x [mm]	y [mm]	dist [mm]
A	0.7	-13.0	13.0	5.7	5.0	7.6	-6.3	8.0	10.2
B	5.3	1.7	5.6	-9.7	-0.3	9.7	4.3	-1.3	4.5
C	-0.7	0.0	0.7	-0.7	0.0	0.7	1.3	0.0	1.3
D	0.3	-2.0	2.0	1.3	1.0	1.7	-1.7	1.0	1.9
E	-0.3	2.0	2.0	2.7	0.0	2.7	-2.3	-2.0	3.1
Avg			4.7			4.4			4.2

Table 4: Halting point coordinates and distance to the origin of the local reference frame for the three AGVs of *Setting* 1.

Operation Points	$R32^{(m)}$			$R30^{(a)}$			$R31^{(a)}$			$R36^{(a)}$		
	x [mm]	y [mm]	dist [mm]	x [mm]	y [mm]	dist [mm]	x [mm]	y [mm]	dist [mm]	x [mm]	y [mm]	dist [mm]
P_1	-2.8	-4.5	5.3	7.3	1.5	7.4	-4.8	-3.5	5.9	0.3	6.5	6.5
P_2	-7.8	-1.5	7.9	5.3	-4.5	6.9	0.3	0.5	0.6	2.3	5.5	5.9
P_3	7.8	6.3	10.0	-5.3	0.3	5.3	-3.3	-0.8	3.3	0.8	-5.8	5.8
P_4	-2.5	1.0	2.7	4.5	-3.0	5.4	-0.5	-2.0	2.1	-1.5	4.0	4.3
P_5	7.3	6.0	9.4	-5.8	0.0	5.8	-2.8	1.0	2.9	1.3	-7.0	7.1
P_6	-7.3	-10.5	12.8	4.8	0.5	4.8	0.8	-1.5	1.7	1.8	11.5	11.6
P_7	2.5	8.5	8.9	-2.5	-2.5	3.5	-2.5	1.5	2.9	2.5	-7.5	7.9
P_8	4.5	8.3	9.4	-5.5	-0.8	5.6	-0.5	0.3	0.6	1.5	-7.8	7.9
P_9	5.0	7.5	9.0	-7.0	-5.5	8.9	2.0	4.5	4.9	0.0	-6.5	6.5
P_{10}	5.0	3.5	6.1	-5.0	-0.5	5.0	0.0	2.5	2.5	0.0	-5.5	5.5
Avg			8.1			5.9			2.7			6.9

Table 5: Halting point coordinates and distance to the origin of the local reference frame for the four AGVs of *Setting* 2.

justed by observing the corresponding AGV motion (e.g. α_F/α_B is changed until straight line is obtained, s_w until the travelled distance corresponds to the expected one, etc.). The estimated calibration parameters of all the AGVs are reported in Table 3. *Setting* 1 tests enable assessment of the precision at the operation point achieved with the proposed calibration method. In *Setting* 2 tests, the manually calibrated robot can be used as a reference for the experiments and enables a comparison with the automatic calibration method.

The operating point coordinates are referred to an inertial reference frame in the environment, but it is difficult to compare each halting point of the AGVs with the nominal operating point. Thus, a marking board has been fixed on the floor near each operation point, oriented approximately according to the expected robot orientation. The halting point of each AGV has been measured according to the local reference frame of the marking board. The origin of the local reference frame is placed in the mean point of the halting points reached by all the AGVs. Tables 4 and 5 illustrate the coordinates of the halting points and their distance to the local frame origin respectively for *Setting* 1 and *Setting* 2. Figure 5 is obtained by overlapping all the AGV halting points expressed w.r.t. their local frame for both *Setting* 1 and

Setting 2.

In the experiments performed in *Setting* 1, points A and B are reached by uneven and high curvature paths that stress the control system, whereas the other points (C, D and E) are approachable through smoother trajectories. The distance of AGV halting positions from the local reference origin is larger for operating points A and B (up to 10 mm). This result was expected since the paths reaching these two points tend to stress the control system. Indeed, halting points immediately after such high curvature path segments are never adopted in actual industrial plants. On the other hand, the difference among the halting points of AGVs in C, D and E is about 5 mm in the worst case and 2 mm on the average (Table 4). The global average distance to the mean point for all five operation points is less than 5 mm.

The results obtained in *Setting* 2 enable comparison of the halting positions of a manually calibrated AGV (R32) and three AGVs calibrated with the proposed approach (R30, R31, R36). The average distance between the halting points and the local reference frame origin is larger for R32 than the other vehicles, as shown in Table 5. In particular, the average distance to the origin of R32 is about 8 mm, whereas the other AGVs calibrated using the proposed method obtain distance values less than 7 mm. The slightly different distribution of halting points of R32 w.r.t. R30, R31 and R36 is more apparent from Figure 5, where it can be observed that halting points of R32 are distributed along all directions. Thus, the proposed automated calibration method obtains a worst-case AGV localization accuracy comparable or better than the accuracy obtained by the best manual calibration, which is assumed to guarantee a position error of about 10 mm in industrial practice.

7. Conclusion

In this paper, we have proposed a calibration method that simultaneously computes the intrinsic and extrinsic parameters of an industrial AGV compliant to the tricycle wheeled robot model. The calibration is performed by computing the parameters better fitting the input commands and the sensor egomotion estimation obtained from the sensor measurements. Two formulations of the calibration problem have been developed. The Standard Tricycle Calibration (STC) problem refers to a five parameter model (the steering offset and driving scale, and three sensor pose coordinates). The Asymmetric Tricycle Calibration (ATC) problem considers a six parameter

model that distinguishes the value of steering offset in forward and backward motion. A closed form solution is provided for STC problem, while the ATC is solved through a one-dimension numerical search. Both methods have been implemented in a PLC-like language used to implement the control software architecture of industrial AGVs. Moreover, the observability property of the method has been formally proved and feasibility conditions on the input trajectory for the estimation have been provided. Experiments have been carried out using real industrial AGVs in a warehouse. The precision of the estimated AGV parameters in repeated calibration trials is at most 0.1° for angular parameters and typically less than 6 mm for position parameters. The accuracy can be improved by a proper selection of the path segments executed by the AGV. Furthermore, AGVs calibrated with the proposed method have shown the ability to stop at the same operation points with a typical accuracy of 10 mm if the control system is not overstressed. To our knowledge, this positioning accuracy is comparable with the accuracy obtained with the best manual calibration in current industrial practice. With the suggested number of trajectory segments, the proposed calibration method takes about 12 minutes instead of one hour or more required by the manual iterative procedure.

The availability of an automatic, fast, and accurate calibration method brings the potential for more frequent recalibration and hence better AGV navigation in real warehouses. In particular, diagnostic procedures monitoring the position accuracy of an AGV could trigger automatic recalibration. As a development of this work, we plan to investigate the calibration problem for other kinematic models of AGV, which are adopted in industrial warehouses.

Acknowledgment

The authors would like to thank professor Marco Locatelli (University of Parma), for several fruitful discussions about optimization techniques suitable for this research.

[1] A. Censi, A. Franchi, L. Marchionni, G. Oriolo, Simultaneous calibration of odometry and sensor parameters for mobile robots, IEEE Trans. on Robotics 29 (2) (2013) 475–492. doi:10.1109/TRO.2012.2226380.

[2] J. Borenstein, L. Feng, Measurement and correction of systematic odom-

etry errors in mobile robots, IEEE Transactions on Robotics and Automation 12 (6) (1996) 869–880. doi:10.1109/70.544770.

[3] T. Larsen, M. Bak, N. Andersen, O. Ravn, Location estimation for an autonomously guided vehicle using an augmented Kalman filter to autocalibrate the odometry, in: First International Conference on Multisource-Multisensor Information Fusion (FUSION'98), 1998.

[4] A. Martinelli, R. Siegwart, Observability Properties and Optimal Trajectories for On-line Odometry Self-Calibration, in: Proc. of the International Conference on Decision and Control, 2006, pp. 3065–3070.

[5] A. Martinelli, N. Tomatis, R. Siegwart, Simultaneous localization and odometry self calibration for mobile robot, Autonomous Robots 22 (1) (2007) 75–85. doi:10.1007/s10514-006-9006-7.

[6] G. Antonelli, S. Chiaverini, G. Fusco, A calibration method for odometry of mobile robots based on the least-squares technique: theory and experimental validation, IEEE Trans. on Robotics 21 (5) (2005) 994–1004. doi:10.1109/TRO.2005.851382.

[7] G. Antonelli, S. Chiaverini, Linear estimation of the physical odometric parameters for differential-drive mobile robots, Journal of Autonomous Robots 23 (1) (2007) 59–68. doi:10.1007/s10514-007-9030-2.

[8] K. Lee, W. Chung, Calibration of kinematic parameters of a Car-Like Mobile Robot to improve odometry accuracy, in: Proc. of the IEEE Int. Conf. on Robotics & Automation (ICRA), 2008, pp. 2546–2551. doi:10.1109/ROBOT.2008.4543596.

[9] M. De Cecco, Self-calibration of AGV inertial-odometric navigation using absolute-reference measurements, in: Proc. IEEE Instrumentation and Measurement Technology Conference (IMTC), Vol. 2, 2002, pp. 1513–1518 vol.2. doi:10.1109/IMTC.2002.1007183.

[10] P. Goel, S. Roumeliotis, G. Sukhatme, Robust localization using relative and absolute position estimates, in: Proc. of the IEEE/RSJ Int. Conf. on Intelligent Robots and Systems (IROS), 1999, pp. 1134–1140. doi:10.1109/IROS.1999.812832.

[11] J. Kang, W.-S. Choi, S.-Y. An, S.-Y. Oh, Augmented EKF based SLAM method for improving the accuracy of the feature map, in: Proc. of the IEEE/RSJ Int. Conf. on Intelligent Robots and Systems (IROS), 2010, pp. 3725–3731. doi:10.1109/IROS.2010.5652938.

[12] E. Foxlin, Generalized architecture for simultaneous localization, auto-calibration, and map-building, in: Proc. of the IEEE/RSJ Int. Conf. on Intelligent Robots and Systems (IROS), Vol. 1, 2002, pp. 527–533. doi:10.1109/IRDS.2002.1041444.

[13] O. Faugeras, G. Toscani, Camera calibration for 3-D computer vision, in: Proc. Int. Work. Industrial Applications of Machine Vision and Machine Intelligence, 1987, pp. 240–247.

[14] P. Liang, Y. Chang, S. Hackwood, Adaptive self-calibration of vision-based robot systems, IEEE Trans. on Systems, Man and Cybernetics 19 (4) (1989) 811–824. doi:10.1109/21.35344.

[15] T. Sasaki, H. Hashimoto, Calibration of laser range finders based on moving object tracking in Intelligent Space, in: Int. Conf. on Networking, Sensing and Control (ICNSC), 2009, pp. 620–625. doi:10.1109/ICNSC.2009.4919349.

[16] J. Song, G.-I. Jee, Kalman filter based on-line calibration of laser scanner for vehicle navigation, in: Control, Automation and Systems (ICCAS), 2011 11th International Conference on, 2011, pp. 1437–1441.

[17] A. Martinelli, D. Scaramuzza, R. Siegwart, Automatic self-calibration of a vision system during robot motion, in: Proc. of the IEEE Int. Conf. on Robotics & Automation (ICRA), 2006, pp. 43–48. doi:10.1109/ROBOT.2006.1641159.

[18] F. Mirzaei, S. Roumeliotis, A Kalman Filter-Based Algorithm for IMU-Camera Calibration: Observability Analysis and Performance Evaluation, IEEE Trans. on Robotics 24 (5) (2008) 1143–1156. doi:10.1109/TRO.2008.2004486.

[19] Z. Zhang, A flexible new technique for camera calibration, IEEE Trans. on Pattern Analysis and Machine Intelligence 22 (11) (2000) 1330–1334. doi:10.1109/34.888718.

[20] R. Tsai, R. Lenz, A new technique for fully autonomous and efficient 3D robotics hand/eye calibration, IEEE Trans. on Robotics and Automation 5 (3) (1989) 345–358. doi:10.1109/70.34770.

[21] R. Horaud, F. Dornaika, Hand-eye Calibration, Int. Journal of Robotics Research 14 (3) (1995) 195–210. doi:10.1177/027836499501400301.

[22] Q. Zhang, R. Pless, Extrinsic calibration of a camera and laser range finder (improves camera calibration), in: Proc. of the IEEE/RSJ Int. Conf. on Intelligent Robots and Systems (IROS), 2004, pp. 2301–2306. doi:10.1109/IROS.2004.1389752.

[23] N. Roy, S. Thrun, Online self-calibration for mobile robots, in: Proc. of the IEEE Int. Conf. on Robotics & Automation (ICRA), Vol. 3, 1999, pp. 2292–2297. doi:10.1109/ROBOT.1999.770447.

[24] A. Kelly, Linearized Error Propagation in Odometry, Int. Journal of Robotics Research 23 (2) (2004) 179–218. doi:10.1177/0278364904041326.

[25] D. Cucci, M. Matteucci, A Flexible Framework for Mobile Robot Pose Estimation and Multi-Sensor Self-Calibration, in: Proc. of the Intl. Conf. on Informatics in Control, Automation and Robotics (ICINCO), pp. 361–368.

[26] J. Underwood, A. Hill, T. Peynot, S. Scheding, Error modeling and calibration of exteroceptive sensors for accurate mapping applications, Journal of Field Robotics 27 (1) (2010) 2–20. doi:10.1002/rob.20315.

[27] J. Brookshire, S. Teller, Automatic calibration of multiple coplanar sensors, in: Robotics: Science and Systems, MIT Press, 2011. doi:10.15607/RSS.2011.VII.005.

[28] J. Brookshire, S. Teller, Extrinsic Calibration from Per-Sensor Egomotion, in: Robotics: Science and Systems, MIT Press, 2012.

[29] B. Siciliano, L. Sciavicco, L. Villani, G. Oriolo, Robotics : modelling, planning and control, Advanced Textbooks in Control and Signal Processing, Springer, London, 2009.

[30] R. Smith, P. Cheeseman, On the representation and estimation of spatial uncertainty, Int. Journal of Robotics Research 5 (4) (1986) 56–68.

[31] H. Hmam, Quadratic optimisation with one quadratic equality constraint, Tech. Rep. DSTO-TR-2416, Electronic Warfare and Radar Division, Defence Science and Technology Organisation (Australia) (2010). URL `http://nla.gov.au/nla.arc-24592`

[32] F. Lu, E. Milios, Robot Pose Estimation in Unknown Environments by Matching 2D Range Scans, in: IEEE Computer Vision and Pattern Recognition Conference (CVPR), 1994, pp. 935–938.

[33] D. Ronzoni, R. Olmi, C. Secchi, C. Fantuzzi, AGV global localization using indistinguishable artificial landmarks, in: Proc. of the IEEE Int. Conf. on Robotics & Automation (ICRA), 2011, pp. 287–292. doi:10.1109/ICRA.2011.5979759.